

## Size-dependent hydrophobic to hydrophilic transition for nanoparticles: A molecular dynamics study

Chi-cheng Chiu,<sup>1</sup> Preston B. Moore,<sup>2</sup> Wataru Shinoda,<sup>3</sup> and Steven O. Nielsen<sup>1,a)</sup>

<sup>1</sup>Department of Chemistry, The University of Texas at Dallas, 800 West Campbell Road, Richardson, Texas 75080, USA

<sup>2</sup>Department of Chemistry and Biochemistry, University of the Sciences in Philadelphia, Philadelphia, Pennsylvania 19104, USA

<sup>3</sup>Research Institute for Computational Sciences, National Institute of Advanced Industrial Science and Technology (AIST), Central 2, 1-1-1, Umezono, Tsukuba, Ibaraki 305-8568, Japan

(Received 31 August 2009; accepted 3 December 2009; published online 28 December 2009)

The physical properties of nanoscale materials often vary with their size, unlike the corresponding bulk material properties, which can only be changed by modifying the material composition. In particular, it is believed that hydration phenomena are length scale dependent. The manifestation of hydrophobicity over multiple length scales plays a crucial role in self-assembly processes such as protein folding and colloidal stability. In the case of particles composed of a bulk hydrophobic material, it is well known that the free energy of hydration monotonically increases with particle size. However, the size-dependent free energy of hydration for particles composed of a bulk hydrophilic material has not been studied. Here we show that the free energy of hydration is not a monotonic function of particle size, but rather, changes sign from positive to negative as the particle size increases. In other words, the particle is hydrophobic at small size and hydrophilic at large size. This behavior arises from a purely geometrical effect caused by the curvature of the particle-water interface. We explore the consequences of this phenomenon on colloidal stability and find that it dictates the shape of colloidal aggregates. © 2009 American Institute of Physics.

[doi:[10.1063/1.3276915](https://doi.org/10.1063/1.3276915)]

### I. INTRODUCTION

The physical properties of nanoscale materials often vary with their size, unlike the corresponding bulk material properties which can only be changed by modifying the material composition. The best known example of this size-dependence is perhaps the fluorescence emission wavelength of semiconductor quantum dots, which has been used to great advantage in multiplexed biological imaging applications.<sup>1,2</sup> Another example is the length scale dependence of hydration phenomena.<sup>3</sup> At the macroscopic level, hydrophobicity is often characterized by the contact angle a water droplet forms on a planar substrate. Using a simple macroscopic thermodynamic analysis based on Young's equation, a hydrophobic surface corresponds to an obtuse contact angle,<sup>4</sup> which in turn corresponds to  $\gamma_\infty > 0$ . Here  $\gamma_\infty$  is the surface tension of the planar water-substrate interface.

Molecular signatures of hydrophobicity have, however, remained elusive. The suggestion that the interface between a large hydrophobic solute and water could resemble a liquid-vapor interface<sup>5</sup> has generated much controversy over the past decade.<sup>6–8</sup> Lum–Chandler–Weeks theory predicts a crossover in the hydration thermodynamics of hydrophobic solutes from a small length scale to a large length scale dependence based on the so-called dewetting transition.<sup>9</sup> However, these simple results apply only for a true hard wall, and predictions about the vapor layer thickness are strongly af-

ected by the presence of even weak attractive interactions between the wall and adjacent water. Complete drying or even the formation of a vapor layer of any significant extent at a single interface is hardly ever relevant in practice.<sup>8</sup> Indeed, Godawat *et al.*<sup>10</sup> reported from extensive simulations of the hydration of interfaces with varying chemistries that the water density near these surfaces provides a poor quantification of surface hydrophobicity. Clues to finding quantitative molecular signatures of hydrophobicity have come from recent simulation studies. Mittal and Hummer<sup>11</sup> show that the interface of large hydrophobic solutes is rough and flickering and broadened by capillary wavelike fluctuations. Giovambattista *et al.*<sup>12,13</sup> show that water confined between hydrophobic plates is more compressible than in bulk water or between hydrophilic surfaces. Godawat *et al.*<sup>10</sup> showed that the probability of cavity formation correlates quantitatively with the macroscopic wetting properties and serves as an excellent signature of hydrophobicity. Specifically, the probability of cavity formation is enhanced in the vicinity of hydrophobic surfaces, and water-water correlations correspondingly display characteristics similar to those near a vapor-liquid interface.<sup>10</sup> A picture of the hydrophobic-water interface that emerges from these studies is that hydration shells of hydrophobic solutes are soft, highly compressible, and characterized by enhanced density fluctuations.<sup>14</sup>

The length scale hydration dependence of hydrophilic solutes has not received nearly the same attention, although it has been suggested that the extent of wetting depends on the strength of the solvent-solute attraction and on the local

<sup>a)</sup>Electronic mail: [steven.nielsen@utdallas.edu](mailto:steven.nielsen@utdallas.edu).

surface curvature.<sup>10,15</sup> This gap in knowledge in such a fundamental area has motivated the present study. To fill this gap we focus explicitly on the role of surface curvature and of attractive interactions. We have chosen to study systems consisting of water and spherical particles, thus having only three interactions: particle-particle, water-water, and particle-water. To connect the hydrophobic and hydrophilic particle scenarios in a seamless and transparent manner, we have chosen simply to vary the particle-water van der Waals interaction strength  $\epsilon$  in a series of simulations. The balance between this energy parameter and the water-water interaction energy determines the value of  $\gamma_\infty$ . That is, for large enough  $\epsilon$ , the planar solid-water interface is hydrophilic ( $\gamma_\infty < 0$ ), whereas for small enough  $\epsilon$ , the planar solid-water interface is hydrophobic ( $\gamma_\infty > 0$ ).<sup>16</sup>

In this study we characterize nanoscale hydrophobicity by positive values of the free energy of hydration. We find that for  $\epsilon$  values corresponding to  $\gamma_\infty < 0$  the particle is hydrophobic for small radii and hydrophilic for large radii, contrary to the case when  $\gamma_\infty > 0$  for which the particles are always hydrophobic regardless of their size. In other words, the solvation free energy is not a monotonic function of particle size, but rather, changes sign from a positive to a negative value as the particle size increases. We show that this behavior arises from a purely geometrical effect caused by the curvature of the particle-water interface. In this sense the phenomenon we report is generic and is not sensitive to any particular choice of force field.

In a similar spirit to our work, Athawale *et al.*<sup>17</sup> calculated the solute size-dependent free energy of hydration over a range of solute-water attractions and plotted the data on a crossover diagram which shows the variation of the effective surface tension of the solute-water interface with solute size. When viewed from the perspective of the length scale dependence of hydrophobicity, there is a significant sensitivity of the solvation free energy to solute-water attractions. Indeed, Ashbaugh and Paulaitis<sup>18</sup> noted that large hard sphere solutes dewet, while methane clusters of the same size do not. Athawale *et al.*<sup>17</sup> observed that the enhancement in water density near large attractive solutes and the corresponding solute-water energy can make the solvation free energy significantly more favorable than for small solutes and even negative in some cases.

Intrigued by this phenomenon, we decided to explore its implications on colloidal stability. Since hydrophobic particles tend to aggregate and hydrophilic particles tend to disperse in water, we hypothesized that small particles should aggregate until they reach some critical size, at which point the aggregate-water interface becomes hydrophilic due to its decreased curvature and stops growing. However, we instead found that the curvature-dependent hydrophobicity/hydrophilicity dictates the shape of colloidal aggregates. When we restricted the shape by assuming spherically coalesced aggregates, we found a critical size beyond which colloidal stability was achieved.

## II. METHODS

### A. Force field

The water-water interaction is modeled using the recent coarse grain force field of Shinoda.<sup>19,20</sup> This model reproduces the experimental liquid-vapor surface tension, which is the most important physical property of the solvent related to our study. However, the conclusions drawn here are general and do not depend on the choice of the force field. The potential energy between water sites is given by  $u_{ll}(r') = 3(3)^{1/2}\epsilon_{ll}/2[(\sigma_{ll}/r')^{12} - (\sigma_{ll}/r')^4]$ , where  $r'$  is the distance between the molecules, and where  $\epsilon_{ll} = 0.895$  kcal/mol,  $\sigma_{ll} = 4.37$  Å.

Since we are not interested in the internal degrees of freedom of the solid particles for this study, we model the particles as continuum spherical solids in analogy to Hamaker's treatment.<sup>21-23</sup> To derive the particle-water interaction, we suppose that  $\rho$  is the number density of interaction sites in the solid particle, and that the van der Waals energy between one of these interaction sites and a liquid site is given by  $u_{pl}(r') = 27\epsilon/4[(\sigma_{pl}/r')^9 - (\sigma_{pl}/r')^6]$ , where  $r'$  is the distance between the sites,  $\epsilon$  is the tunable particle-water interaction strength, and  $\sigma_{pl} = 4.0$  Å. The Lennard-Jones 9-6 functional form used here is typical of coarse grain force fields.<sup>19,20</sup> The potential energy between a single water site and the entire solid particle is then obtained by integrating over the continuum solid,  $U = \int_V \rho u_{pl} dV$ , where  $V$  is the volume of the particle. Without loss of generality, we can place the particle at the origin and the water site at  $(0, 0, R)$ . An interaction site in the solid is located at position  $(a \sin \phi \cos \theta, a \sin \phi \sin \theta, a \cos \phi)$ , so that the integral can be written explicitly as

$$U = \int_0^r \int_0^{2\pi} \int_0^\pi a^2 \sin \phi \rho u_{pl}(\xi) d\phi d\theta da, \quad (1)$$

where  $r$  is the particle radius,  $R$  is the distance between the particle center and a water molecule, and  $\xi^2 = a^2 - 2aR \cos \phi + R^2$ .

The integration can be performed analytically, yielding

$$U(R, r) = \frac{9\pi\epsilon\rho\sigma_{pl}^9 r^3 (3r^4 + 42r^2 R^2 + 35R^4)}{35R(R^2 - r^2)^6} - \frac{9\pi\epsilon\rho\sigma_{pl}^6 r^3}{(R^2 - r^2)^3}. \quad (2)$$

We take  $\rho = 0.113/3$  Å<sup>-3</sup> which is a factor of three smaller than the atomic number density used below because the coarse grained water particle is composed of three water molecules.<sup>22,23</sup> Notice that  $\epsilon$  and  $\rho$  appear simply as linear factors in Eq. (2); choosing a different value for  $\rho$  yields the same potential  $U(R, r)$  if  $\epsilon$  is rescaled appropriately.

The form of the potential  $U(R, r)$  is shown in Fig. 1 for different  $r$  values with  $\epsilon = 0.442$  kcal/mol. The minimum of the potential is at approximately  $(r + 3.3$  Å). The "extra" 3.3 Å is due to the excluded volume (Pauli repulsion) between an interaction site in the solid particle and a liquid site. The depth of the minimum converges to  $-3.27$  kcal/mol as  $r \rightarrow \infty$ , which corresponds to a planar solid-water interface. The reduction of the well depth at finite  $r$  is purely a geometrical effect caused by the curvature of the particle-water

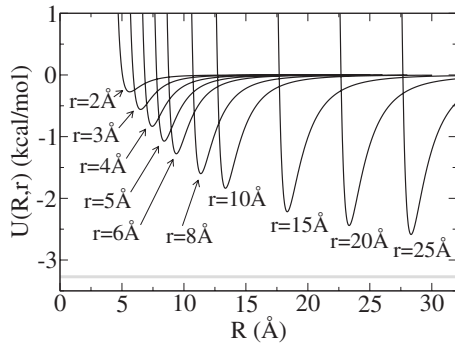


FIG. 1. Particle-water potential energy for  $\epsilon=0.442$  kcal/mol. The minimum of the potential is at approximately ( $r+3.3$  Å). The depth of the minimum converges to  $-3.27$  kcal/mol as  $r \rightarrow \infty$ , shown in horizontal gray line.

interface. As mentioned previously, this geometrical effect is responsible for the phenomena whereby a particle can change in character from hydrophobic to hydrophilic as its size increases.

Next, we derive the particle-particle interaction for use in our colloid studies. This interaction is simply that of two continuum solids as was considered many years ago by Hamaker.<sup>21</sup> The particle-particle potential energy is given by

$$U_{PP} = \int_{V_1} \int_{V_2} u_{pp} \rho_1 \rho_2 dV_1 dV_2, \quad (3)$$

where  $\rho_1$  and  $\rho_2$  are the number density of atoms in the two particles,  $V_1$  and  $V_2$  are the volumes of the two particles, and  $u_{pp}(r') = 4\epsilon_{pp}[(\sigma_{pp}/r')^{12} - (\sigma_{pp}/r')^6]$  is the atom-atom van der Waals interaction between an atom in one particle and an atom in the other particle a distance  $r'$  apart from one another. This integral is straightforward to evaluate, yielding

$$U_{PP}(d,r) = \frac{64\pi^2 \rho_1 \rho_2 \epsilon_{pp} \sigma_{pp}^{12} r^6 P(d,r)}{4725 d^7 (2r+d)^8 (4r+d)^7} + \frac{2\pi^2 \rho_1 \rho_2 \epsilon_{pp} \sigma_{pp}^6}{3} \left[ \frac{r}{2} \left( \frac{1}{4r+d} - \frac{1}{d} \right) - \frac{4r}{(2r+d)^2} + \log \frac{(2r+d)^2}{d(4r+d)} \right], \quad (4)$$

where  $P(d,r) = 525d^{10} + 10\,500rd^9 + 93\,660r^2d^8 + 490\,560r^3d^7 + 167\,445\,6r^4d^6 + 391\,171\,2r^5d^5 + 637\,683\,2r^6 \times d^4 + 720\,025\,6r^7d^3 + 539\,238\,4r^8d^2 + 241\,664\,0r^9d + 491\,520r^{10}$ . In Eq. (4) we have specialized to the case of two identical particles of equal radii  $r$ , where the closest distance between the two particles is  $d$ , so that the center of mass separation of the two particles from one another is given by  $d+2r$ . The  $\sigma_{pp}^6$  attractive term in Eq. (4) is identical to Eq. 39 of Adamczyk,<sup>24</sup> while the  $\sigma_{pp}^{12}$  repulsive term has not previously been reported to our knowledge. We have used  $\rho_1 = \rho_2 = 0.113$  Å<sup>-3</sup>,  $\epsilon_{pp} = 0.07$  kcal/mol, and  $\sigma_{pp} = 3.55$  Å.<sup>22,23</sup>

The only parameters we vary for the simulation studies are  $r$ , the particle radius and  $\epsilon$ , the particle-water interaction strength.

## B. Molecular dynamics simulation methods

We employ three-dimensional periodic boundary condition for all systems. We use the Nosé–Hoover chain method of length 5 to control the temperature to 303.15 K.<sup>25</sup> We use an Andersen barostat to control the pressure to 0.1 MPa.<sup>26</sup> Integration of the equations of motion is carried out using the reversible RESPA algorithm.<sup>27</sup> Specifically, a force-based splitting of the time step is used: the time step size for updating the long-range nonbonded force is 30 fs and that for the short-range nonbonded forces is 3 fs (there are only van der Waals forces present for all of the systems considered here). All of the simulations were carried out using MPDYN.<sup>28</sup>

## C. Solvation free energy method

To compute the solvation free energy  $G(r)$  shown in Fig. 3, we employed our novel free energy method.<sup>29,30</sup> Specifically, we computed the mean force of constraint on the particle radius due to all the solvent molecules during an equilibrium molecular dynamics simulation,  $F(r) \equiv \langle \sum_i \partial U(R_i, r) / \partial r \rangle$ , where  $R_i$  indexes the distance between solvent molecule  $i$  and the particle. We then computed the solvation free energy of the particle using thermodynamic integration,  $G(r) = \int_0^r F(\xi) d\xi$ . For each of the 11 values of  $\epsilon$  shown in Fig. 3, we performed equilibrium simulations with particles of radii 0.15, 0.5, 1.0, 2.0, 3.0, 4.0, 5.0, 6.0, 7.0, 8.0, and 9.0 Å in unit cells with between 5000 and 10000 water sites. For  $\epsilon=0.442$  kcal/mol, we performed 14 additional simulations with radii 10.0, 11.0, 12.0, ..., 21.0, 22.0, and 23.0 Å with between 10 000 and 30 000 water sites. Each of the 135 simulations was run for 10 ns.

## D. Colloid simulation methods

To investigate the aggregation phenomenon suggested from the data shown in Fig. 3, we need to define a criterion for particle aggregation (cluster formation). We define a cluster of  $n$  particles as an  $n$ -body path-connected set. Namely, any two particles  $i$  and  $j$  in the cluster must be connected to each other by a path of one or more steps beginning at particle  $i$  and ending at particle  $j$  with each step being between two particles in the cluster separated from each other by a distance of less than a threshold value of  $d_*$ . This definition imposes no constraints on the shape of the cluster which has been seen to be important in nucleation theory,<sup>31</sup> i.e., we do not constrain the cluster to be spherical or linear or any particular shape, and it can adopt any shape as long as the  $n$  particles are connecting within the cluster.

During a molecular dynamics simulation of a cluster of  $n$  particles, we ensure the cluster is kept intact with the following algorithm: At each time step of the simulation, we chose one of the  $n$  particles and created a cluster list, called list A, containing, initially, only this particle. We placed the remaining  $(n-1)$  particles in another list, called list B. Then, we identified the minimum particle-particle distance  $d$  between the two lists, namely, the minimum particle-particle distance where one particle is restricted to belong to list A, and the other particle is restricted to belong to list B. We applied a cluster constraint force between these two particles based on the potential energy function

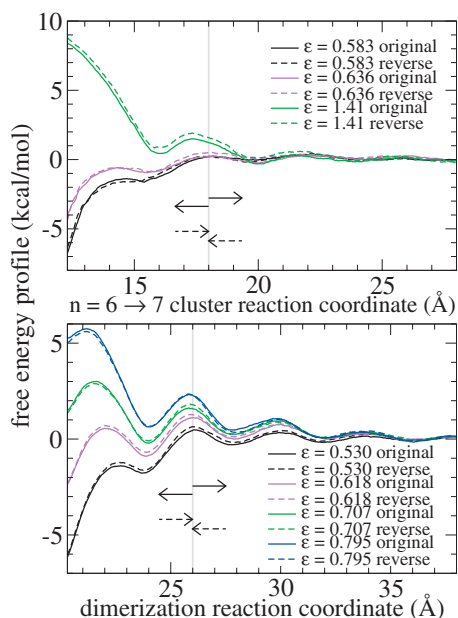


FIG. 2. Representative free energy profiles demonstrating quasiequilibrium for the steered MD simulations performed in this study. Each free energy profile is computed from a pair of simulations, labeled “original” and shown in solid line, by pulling in opposite directions from a common reaction coordinate value. At the termini of this pair of runs, the resulting system coordinates and velocities are subjected to steered MD simulations with the reverse pulling velocity, labeled “reverse” and shown in dashed line. The top panel shows data for the 6  $\rightarrow$  7 cluster study, and the bottom panel shows data for the  $r=9$  Å dimerization study ( $\epsilon$  in kcal/mol in both panels).

$$U_{\text{cluster}}(d) = \begin{cases} 0 & \text{if } d < d_* \\ k_{\text{cluster}}(d - d_*)^3 & \text{if } d > d_* \end{cases} \quad (5)$$

where  $d$  is the distance between the two particles. We then transferred the particle in list B to which this force was applied to list A, and repeated the process until list A contained  $n$  particles and list B was empty. For the  $r=5$  Å particles used here, we took  $k_{\text{cluster}}=20$  kcal/mol/Å<sup>3</sup> and  $d_* = 12.3$  Å.

The  $n \rightarrow (n+1)$  cluster addition free energy  $\Delta G$  shown in Fig. 5 is computed as follows. While imposing the cluster constraint on a preselected set of  $n$  particles, we performed two “slow growth” simulations starting from a configuration where the  $(n+1)$ <sup>st</sup> particle is 18 Å away from the nearest cluster particle. In one simulation we pulled the  $(n+1)$ <sup>st</sup> particle toward the cluster at a speed of 0.15 Å/ns, until it was a distance  $d_*$  from the nearest cluster particle (approximately 40 ns). In the other simulation, we pulled the  $(n+1)$ <sup>st</sup> particle away from the cluster at a speed of 0.40 Å/ns for 25 ns, at which point it is no longer interacting with the cluster. We used a slightly faster speed when pulling away from the cluster since the interaction with the cluster over this distance range is weak. The  $n \rightarrow (n+1)$  cluster addition free energy  $\Delta G$  is given by the free energy difference between the endpoints of these two pulling runs and was conducted in a cubic cell containing 2000( $n+1$ ) water sites. We confirmed that these simulations were at quasiequilibrium by reversing the pulling direction in the final restart file for a few of the systems, which will show hysteresis if the system has been perturbed away from equilibrium;<sup>32</sup> some of this data is shown in the top panel of Fig. 2. The force constant for the

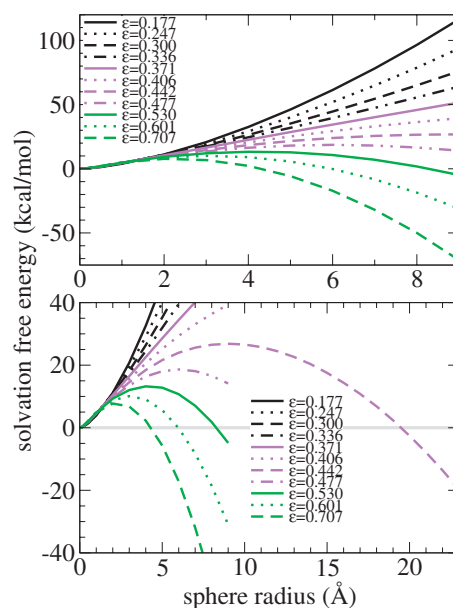


FIG. 3. The solvation free energy  $G(r)$  as a function of the particle radius  $r$  for different values of the particle-water interaction strength  $\epsilon$  (given in kcal/mol). For each  $r$  value,  $G(r)$  for  $\epsilon_1$  is greater than  $G(r)$  for  $\epsilon_2$  if  $\epsilon_1 < \epsilon_2$ . The two panels show the same data on different scales.

constant velocity pulling harmonic constraint was 50 kcal/mol/Å<sup>2</sup>.

To compute the mean number of contacts in each cluster shown in Fig. 7, we took the assembled clusters from the cluster addition free energy study and ran them for another 20 ns in the presence of the cluster constraint force given in Eq. (5). A (self-)contact is defined to exist if the distance between two particles is less than 12.75 Å.<sup>33</sup>

The dimerization free energies shown in Fig. 8 were computed from pairs of slow growth steered molecular dynamics simulations as described above, but this time with the same inwards and outwards pulling velocity of 0.1 Å/ns. For the dimerization studies, we also confirmed that these simulations were at quasiequilibrium by reversing the pulling direction in the final restart file for the 9 Å particle systems; the data are shown in the bottom panel of Fig. 2. We used 5000, 7000, 9000, 11 000, 13 000, and 16 000 water sites, respectively, for the  $r=5$  Å,  $r=7$  Å,  $r=9$  Å,  $r=11$  Å,  $r=13$  Å, and  $r=15$  Å dimerization simulations.

### III. SINGLE-PARTICLE SOLVATION FREE ENERGY

The nanoparticle solvation excess free energy  $G(r)$ , defined as the free energy cost of transferring a solid spherical particle of radius  $r$  from an ideal gas reference state into water, is obtained by thermodynamic integration of  $(\partial G/\partial r)_{N,P,T}$  as described in Sec. II. The nanoparticle solvation free energy  $G(r)$  is seen in Fig. 3 to be roughly a quadratic function of  $r$ . In the limit of  $r \rightarrow \infty$  the excess free energy of solvation per unit surface area converges to the surface tension  $\gamma_\infty$  of the corresponding planar solid-water interface.<sup>34</sup> The surface tension of the planar interface can be calculated from molecular dynamics simulations either by extrapolating the finite radius  $G(r)$  data, through  $\gamma_\infty = \lim_{r \rightarrow \infty} G(r)/(4\pi(r+\delta)^2)$ , or independently from the simu-

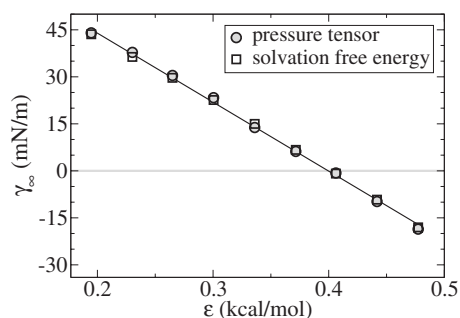


FIG. 4. The planar ( $r \rightarrow \infty$  limit) particle-water surface tension is plotted as a function of the particle-water interaction strength  $\epsilon$ . The conventional pressure tensor approach and the extrapolated solvation free energy approach are seen to be in excellent agreement.

lation of a planar interface as discussed in detail by Vázquez<sup>29</sup> through the difference of pressure tensor components normal and tangential to the interface  $\gamma_\infty = L_\perp(P_\parallel - P_\perp)$ .<sup>35,36</sup> The agreement between these two methods is shown in Fig. 4. The choice of  $\delta$ , which corresponds to different solute-solvent dividing surfaces, is not important for the present study because we are primarily concerned with  $G(r)$  and  $\gamma_\infty$ , neither of which depend on  $\delta$ .

It is clear from Fig. 4 that  $\gamma_\infty > 0$  for solid-water interaction strengths of  $\epsilon < 0.40$  kcal/mol, and  $\gamma_\infty < 0$  for  $\epsilon > 0.40$  kcal/mol. In other words, in the limit  $r \rightarrow \infty$ ,  $\epsilon > 0.40$  kcal/mol corresponds to a macroscopically hydrophilic material, and for  $\epsilon < 0.40$  kcal/mol to a macroscopically hydrophobic material.<sup>37</sup> For a macroscopically hydrophobic material,  $G(r)$  is a monotone increasing function of  $r$ .<sup>3</sup> However, the behavior of  $G(r)$  for particles made of macroscopically hydrophilic material has not previously been reported to our knowledge. Interestingly, we find that for  $\epsilon$  values corresponding to  $\gamma_\infty < 0$  the particle is hydrophobic for small radii and hydrophilic for large radii, contrary to the case when  $\gamma_\infty > 0$  for which the particles are always hydrophobic regardless of their size. This result can be inferred from the work of Athawale *et al.*<sup>17</sup> in which the solute size-dependent free energy of hydration was calculated for methane, C60, and C180 solutes for different solute-water attraction energies. For the largest attraction energy considered, the hydration free energy is positive for methane and negative for C60 and C180, whereas for small solute-water energies all the solutes were found to have positive hydration free energies.<sup>17</sup> It is clear from Fig. 3 that the hydrophobic to hydrophilic transition is a function of  $\epsilon$  as well as  $r$ , and that for  $\epsilon$  close to 0.40 kcal/mol (corresponding to  $\gamma_\infty = 0$ ) the transition occurs at very large particle size. On the other hand, as mentioned in Sec. II, the water-particle potential energy scales linearly with both  $\epsilon$  and  $\rho$ . Thus the hydrophobic to hydrophilic transition as a function of  $\epsilon$  can be regarded as a function of  $\rho$  at fixed  $\epsilon$ . In other words, the particle changes from hydrophobic to hydrophilic as  $\rho$  increases. This trend was also observed by Choudhury,<sup>15</sup> who showed that the wetting behavior between two hydrophobic plates varies with the site density  $\rho$  of the plates.

This size-dependent hydrophobic to hydrophilic transition is driven by the curvature of the particle-water interface. A water molecule residing close to the interface interacts

with both the particle and with other water molecules. As the particle curvature decreases (corresponding to increasing particle radius) this water molecule experiences an increased interaction energy with the particle and a commensurate decreased interaction energy with other water molecules. The increasing strength of the particle-water interaction (at fixed  $\epsilon$ ) is purely due to the curvature of the interface, as shown in Fig. 1. The resulting curvature-dependent shift in interaction energy between water-particle and water-water is precisely the cause of the observed hydrophobic to hydrophilic transition. For materials that are only macroscopically marginally hydrophilic the crossover occurs at very large radii. For a macroscopically hydrophobic material, the water-particle interface is unfavorable for any particle size, and the free energy cost of the interface only increases with particle size (see Fig. 3).

#### IV. THEORY OF SELF-ASSEMBLY OF SOLID SPHERES IN WATER

We wish to explore the consequences of our observation from Fig. 3 that particles are hydrophobic for small radii and hydrophilic for large radii for certain values of the particle-water interaction strength  $\epsilon$ . This observation leads us to hypothesize a self-assembly mechanism: small particles should aggregate until they look, to the solvent, like a large particle at which point the aggregation will stop. In other words, small particles should cluster until the solvent-particle aggregate curvature is too low.

To flesh out the theoretical basis behind this idea, consider  $n$  spheres in water, each of radius  $r$ . Each sphere has surface area  $4\pi r^2$  and volume  $4\pi r^3/3$ . If these  $n$  spheres aggregate to form a larger spherical assembly, the radius of the assembly is roughly  $R = n^{1/3}r$  and its surface area is  $4\pi R^2$ . Let us assume that the excess free energy of solvation per unit surface area is  $G(r)/4\pi r^2 = \gamma_\infty + ar^{-1}$ , where  $\gamma_\infty$  is the surface tension for the planar solid-water interface. This functional form was also used by Huang.<sup>34</sup> Then, by considering  $n$  monomers versus one large aggregate, the crossover in stability occurs when

$$4\pi n r^2 (\gamma_\infty + ar^{-1}) = 4\pi n^{2/3} r^2 (\gamma_\infty + an^{-1/3} r^{-1}). \quad (6)$$

Let  $x = n^{1/3}$  to give

$$x^2 (\gamma_\infty + ar^{-1}) = x \gamma_\infty + ar^{-1}. \quad (7)$$

Using the quadratic formula to solve for  $n$  gives

$$n = - \left( \frac{\gamma_\infty r}{a} + 1 \right)^{-3}. \quad (8)$$

For  $n > 1$  we have the condition

$$-\frac{2a}{r} < \gamma_\infty < -\frac{a}{r}. \quad (9)$$

This should serve as a rough guide for what parameters to choose to observe this self-assembly mechanism. Namely, we should choose  $r$  and  $\epsilon$  ( $\gamma_\infty$  is controlled by  $\epsilon$  as illustrated in Fig. 4) to obtain conditions favorable for self-assembly. It is clear from Figs. 3 and 4 that for  $\epsilon < 0.40$  kcal/mol the solvation free energy is always positive, meaning that it is

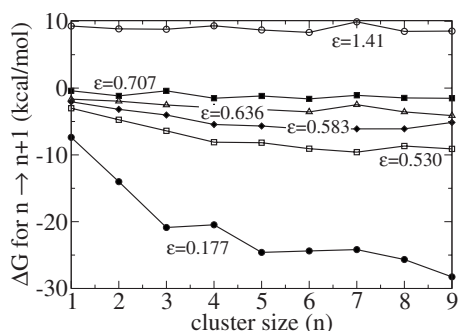


FIG. 5. Free energy of adding one particle to a cluster of  $n$  particles, as a function of  $n$  and of the particle-water interaction strength  $\epsilon$ .

unfavorable to introduce the particle into water and we should expect uncontrolled aggregation, i.e., complete phase separation between the particles and water. For  $\epsilon > 0.40$  kcal/mol the solvation free energy changes sign at some value of the particle size, thus the aggregate should increase until its size is roughly this value.

It should be noted that this analysis is too simple. It ignores the entropy loss upon aggregation (and the entropy change of the solvent) and the particle-particle potential energy; however, these factors partially cancel each other. We also assumed that all the particles were the same size, that they did not change identity by coalescing, and that the aggregate was spherical.

## V. CLUSTER STUDIES

To explore the self-assembly process outlined above, we performed  $n \rightarrow (n+1)$  cluster growth simulations in which we computed the free energy change to increase the size of an  $n$ -particle cluster by one particle. We define a cluster as described in Sec. II. Our definition imposes no constraints on the shape of the cluster which has been seen to be important in nucleation theory.<sup>31</sup>

The results are shown in Fig. 5 for particles of radius  $r = 5$  Å. We chose a particle radius of  $r = 5$  Å because it is clear from the data in Fig. 3 that the phenomenon we wish to explore exists for essentially any desired particle size (by changing  $\epsilon$ ), and  $r = 5$  Å makes the free energy simulations tractable in terms of the number of water molecules needed in the unit cell.

For  $\epsilon = 0.177$  kcal/mol the particles are hydrophobic for any size (since we are below the  $\epsilon = 0.40$  kcal/mol threshold), and tend to aggregate to maximize their self-contacts. As a consequence, the  $n \rightarrow (n+1)$  cluster growth free energy becomes increasingly negative as the cluster grows, because more contacts per particle can be made for a larger cluster. For example, a two-particle cluster can make a maximum of one contact per particle, whereas a three-particle cluster can have two contacts per particle in a triangular geometry, and a four-particle cluster can make three contacts per particle in a tetrahedral geometry. This explains why the cluster growth free energy has a constant slope for  $\epsilon = 0.177$  kcal/mol for the  $1 \rightarrow 2$ ,  $2 \rightarrow 3$ , and  $3 \rightarrow 4$  particle clusters. This trend cannot continue for a five particle cluster due to geometrical limitations on the maximum number of contacts per particle.

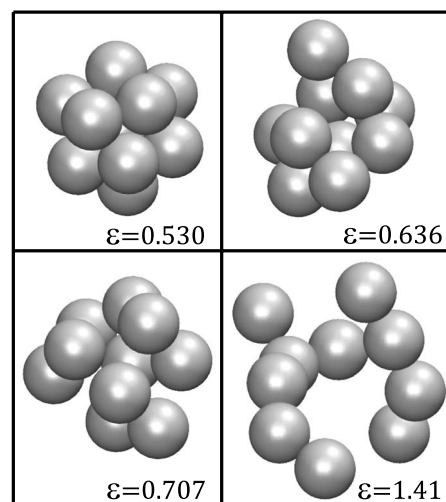


FIG. 6. Representative snapshots of a ten-particle cluster with different particle-water interaction strengths  $\epsilon$ .

Conversely, for  $\epsilon = 1.41$  kcal/mol, the  $r = 5$  Å particle is already hydrophilic, and the free energy to add one particle to the cluster always has the same positive (unfavorable) value. We can understand this by realizing that the particles do not want to aggregate. Instead, they form a linear (or branched) chain which minimizes contacts between particles (see Fig. 6) and maximizes contacts to the solvent. The  $(n+1)$ <sup>st</sup> particle simply attaches to the end of the chain formed by the first  $n$  particles, so that the free energy of cluster growth is roughly constant: essentially the  $(n+1)$ <sup>st</sup> particle only interacts with one particle of the cluster.

For the intermediate values of  $\epsilon = 0.530$ ,  $0.583$ ,  $0.636$ , and  $0.707$  kcal/mol shown in Fig. 5, notice that the dimerization free energy  $n = 1 \rightarrow 2$  is negative. Consequently, we will never see the free energy go to a positive value for any cluster size because of our shape-flexible cluster definition. When we bring another particle to join the cluster, the cluster will rearrange itself to take advantage of the favorable dimerization energy, so that the free energy will always decrease. The fact that the cluster addition free energy is more or less flat for  $\epsilon = 0.707$  kcal/mol is a good indication that the particles are not making many self-contacts (see Fig. 7).

Representative snapshots of the ten-particle clusters are shown in Fig. 6. The mean number of self-contacts for a particle in a cluster is quantified using equilibrium cluster

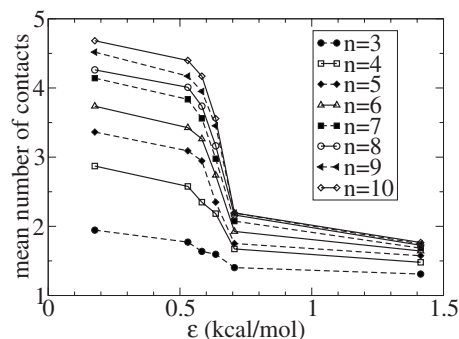


FIG. 7. Mean number of contacts for a particle in an  $n$ -particle cluster, as a function of the particle-water interaction strength  $\epsilon$ .

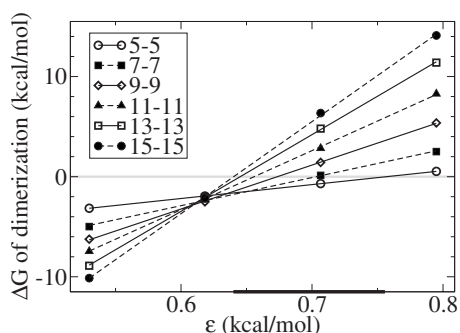


FIG. 8. Dimerization free energy  $\Delta G$  for two equal radius ( $r$  labeled in angstroms in the inset) nanoparticles. Notice that for  $0.64 \text{ kcal/mol} < \epsilon < 0.76 \text{ kcal/mol}$ , there is a transition from  $\Delta G < 0$  to  $\Delta G > 0$  as the particle size increases.

simulations and is summarized in Fig. 7. These data clearly shows a transition from compact to elongated clusters for  $\epsilon > 0.65 \text{ kcal/mol}$ .

## VI. DIMERIZATION STUDIES

The results of the cluster simulation studies are heavily influenced by the shape-flexibility of the cluster definition we used. However, the conceptual idea we developed assumed a spherical cluster shape. There is, of course, a very simple way to stop the cluster from changing shape when we add a particle to it: coalesce the cluster and the additional particle into a single, larger (spherical) particle. In this process the particles do not retain their individuality the way we assumed in the cluster studies.

Here we consider the simplest case, namely, we assume we have two coalesced particles of the same radius  $r$ , and we ask what their dimerization free energy is, as a function of  $r$ . The results are shown in Fig. 8. For  $\epsilon < 0.62 \text{ kcal/mol}$ , we will have uncontrolled aggregation because the dimerization free energy is negative for all particle sizes. Conversely, for  $\epsilon > 0.80 \text{ kcal/mol}$ , we will not observe any aggregation because the dimerization free energy is positive for all particle sizes. However, in a special window of  $\epsilon$  values between these two limiting cases, we observe that the dimerization free energy is negative for small particles and positive for large particles. In other words, it is favorable for small particles to aggregate and then coalesce to form a large particle, which will in turn aggregate and then coalesce up until some critical size at which point aggregation is no longer favorable. This is the behavior we hypothesized should occur on the basis of the solvation free energy data shown in Fig. 3 and our simple theoretical picture.

## VII. CONCLUSIONS

For solid spherical nanoparticles composed of macroscopically hydrophilic material (namely, the particle-water surface tension is negative in the limit of infinite particle size), we demonstrated that the solvation free energy changes sign from a positive to a negative value as the particle size increases. In other words, the particle is hydrophobic at small size and hydrophilic at large size. We showed that this behavior arises from a purely geometrical effect caused by the

curvature of the particle-water interface. By using a continuum model for the spherical nanoparticle, our method incorporates the effect of water-particle interaction strength and site density within the nanoparticle on the hydrophobicity, which is consistent with previous studies. In this sense the phenomenon is generic and is not sensitive to any particular choice of force field.

Based on this observation, we developed a simple theoretical picture which led us to hypothesize a novel self-assembly mechanism. In this mechanism, small hydrophobic particles would cluster together until the aggregate curvature decreased beyond a threshold value, at which point the aggregate would stabilize and stop growing due to the curvature-dependence of the solvation free energy. In other words, small particles should cluster until the solvent-particle aggregate curvature is too low.

However, our attempts to observe this phenomenon failed when we employed a shape-flexible cluster definition. The reason is straightforward. If the dimerization free energy is negative, particles will always join the cluster, but the cluster may rearrange to form a linear (or branched) chain, which minimizes contacts between particles.

When we prevented shape-flexibility by studying the dimerization free energy between two coalesced spherical aggregates, we found that there is a range of particle-water interaction energies for which small particles aggregate but large particles do not. Thus, it is favorable for small particles to aggregate (or coalesce) up until some critical size, at which point it is no longer favorable for the aggregate to keep growing. In this treatment, we ignored the entropic contribution of each original particle because the aggregate is treated as a single point particle. In this sense, we observed a different scenario for the aggregation processes. However, these results clearly tell us that we can have a stable spherical colloid particle with a suitable choice of the size, even though smaller colloid particles made from the same material are unstable (they will aggregate). This finding gives valuable insight into colloidal design.

## ACKNOWLEDGMENTS

S.O.N. acknowledges the Donors of the American Chemical Society Petroleum Research Fund for partial support of this research. P.B.M. acknowledges NSF for Grant Nos. CHE-0420556 and CCF-0622162 for partial support of this research. W.S. is grateful for the support of the Next Generation Super Computing Project, Nanoscience Program, MEXT, Japan.

<sup>1</sup>M. Y. Han, X. H. Gao, J. Z. Su, and S. Nie, *Nat. Biotechnol.* **19**, 631 (2001).

<sup>2</sup>X. Michalet, F. F. Pinaud, L. A. Bentolila, J. M. Tsay, S. Doose, J. J. Li, G. Sundaresan, A. M. Wu, S. S. Gambhir, and S. Weiss, *Science* **307**, 538 (2005).

<sup>3</sup>S. Rajamani, T. M. Truskett, and S. Garde, *Proc. Natl. Acad. Sci. U.S.A.* **102**, 9475 (2005).

<sup>4</sup>X. Huang, C. J. Margulis, and B. J. Berne, *Proc. Natl. Acad. Sci. U.S.A.* **100**, 11953 (2003).

<sup>5</sup>F. H. Stillinger, *J. Solution Chem.* **2**, 141 (1973).

<sup>6</sup>P. Ball, *Chem. Rev. (Washington, D.C.)* **108**, 74 (2008).

<sup>7</sup>H. S. Ashbaugh and L. R. Pratt, *Rev. Mod. Phys.* **78**, 159 (2006).

<sup>8</sup>B. J. Berne, J. D. Weeks, and R. Zhou, *Annu. Rev. Phys. Chem.* **60**, 85

- (2009).
- <sup>9</sup>K. Lum, D. Chandler, and J. D. Weeks, *J. Phys. Chem. B* **103**, 4570 (1999).
- <sup>10</sup>R. Godawat, S. N. Jamadagni, and S. Garde, *Proc. Natl. Acad. Sci. U.S.A.* **106**, 15119 (2009).
- <sup>11</sup>J. Mittal and G. Hummer, *Proc. Natl. Acad. Sci. U.S.A.* **105**, 20130 (2008).
- <sup>12</sup>N. Giovambattista, P. J. Rossky, and P. G. Debenedetti, *Phys. Rev. E* **73**, 041604 (2006).
- <sup>13</sup>N. Giovambattista, C. F. Lopez, P. J. Rossky, and P. G. Debenedetti, *Proc. Natl. Acad. Sci. U.S.A.* **105**, 2274 (2008).
- <sup>14</sup>S. Sarupria and S. Garde, *Phys. Rev. Lett.* **103**, 037803 (2009).
- <sup>15</sup>N. Choudhury, *J. Phys. Chem. B* **112**, 6296 (2008).
- <sup>16</sup>Note that there is no restriction on the sign of the solid-water surface tension; see, for example, F. Leroy, D. J. V. A. dos Santos, and F. Müller-Plathe, *Macromol. Rapid Commun.* **30**, 864 (2009).
- <sup>17</sup>M. V. Athawale, S. N. Jamadagni, and S. Garde, *J. Chem. Phys.* **131**, 115102 (2009).
- <sup>18</sup>H. S. Ashbaugh and M. E. Paulaitis, *J. Am. Chem. Soc.* **123**, 10721 (2001).
- <sup>19</sup>W. Shinoda, R. DeVane, and M. L. Klein, *Mol. Simul.* **33**, 27 (2007).
- <sup>20</sup>W. Shinoda, R. DeVane, and M. L. Klein, *Soft Matter* **4**, 2454 (2008).
- <sup>21</sup>H. C. Hamaker, *Physica (Amsterdam)* **4**, 1058 (1937).
- <sup>22</sup>S. O. Nielsen, G. Srinivas, C. F. Lopez, and M. L. Klein, *Phys. Rev. Lett.* **94**, 228301 (2005).
- <sup>23</sup>S. O. Nielsen, G. Srinivas, and M. L. Klein, *J. Chem. Phys.* **123**, 124907 (2005).
- <sup>24</sup>Z. Adamczyk and P. Weroński, *Adv. Colloid Interface Sci.* **83**, 137 (1999).
- <sup>25</sup>G. J. Martyna, M. L. Klein, and M. Tuckerman, *J. Chem. Phys.* **97**, 2635 (1992).
- <sup>26</sup>G. J. Martyna, D. J. Tobias, and M. L. Klein, *J. Chem. Phys.* **101**, 4177 (1994).
- <sup>27</sup>M. Tuckerman, B. J. Berne, and G. J. Martyna, *J. Chem. Phys.* **97**, 1990 (1992).
- <sup>28</sup>W. Shinoda and M. Mikami, *J. Comput. Chem.* **24**, 920 (2003).
- <sup>29</sup>U. O. M. Vázquez, W. Shinoda, P. B. Moore, C.-c. Chiu, and S. O. Nielsen, *J. Math. Chem.* **45**, 161 (2009).
- <sup>30</sup>R. J. B. Kalescky, W. Shinoda, P. B. Moore, and S. O. Nielsen, *Langmuir* **25**, 1352 (2009).
- <sup>31</sup>S. Auer and D. Frenkel, *Nature (London)* **409**, 1020 (2001).
- <sup>32</sup>S. Park, F. Khalili-Araghi, E. Tajkhorshid, and K. Schulten, *J. Chem. Phys.* **119**, 3559 (2003).
- <sup>33</sup>We redid the self-contact analysis for slightly different distance choices, including the value of  $d_* = 12.3$  Å. The absolute numbers change a little but the trends in the data remain unchanged.
- <sup>34</sup>D. M. Huang, P. L. Geissler, and D. Chandler, *J. Phys. Chem. B* **105**, 6704 (2001).
- <sup>35</sup>M. P. Allen and D. J. Tildesley, *Computer Simulations of Liquids* (University Press, Oxford, 1992).
- <sup>36</sup>D. Frenkel and B. Smit, *Understanding Molecular Simulation* (Academic, New York, 2002).
- <sup>37</sup>N. Giovambattista, P. G. Debenedetti, and P. J. Rossky, *J. Phys. Chem. B* **111**, 9581 (2007).